

# Microscale Location, Characterization, and Association of Polycyclic Aromatic Hydrocarbons on Harbor Sediment Particles

UPAL GHOSH,<sup>†</sup> J. SEB GILLETTE,<sup>‡</sup>  
RICHARD G. LUTHY,<sup>\*,†</sup> AND  
RICHARD N. ZARE<sup>‡</sup>

*Department of Civil and Environmental Engineering  
and Department of Chemistry, Stanford University,  
Stanford, California 94305-4020*

Complementary mass spectrometric and spectroscopic techniques were employed to provide direct information at the microscale on the sequestration of polycyclic aromatic hydrocarbon (PAH) contaminants in Milwaukee Harbor sediment particles. Microprobe two-step laser desorption/laser ionization mass spectrometry was used for PAH measurements, infrared microspectroscopy was used for organic carbon measurement, and scanning electron microscopy with wavelength dispersive X-ray spectroscopy was used for elemental microanalysis. PAH concentrations on coal- and wood-derived particles were found to be several orders of magnitude higher than on silica particles. A cryomicrotome sectioning procedure was employed for particle cross-sectional investigations, and it was found that most PAHs are concentrated on external surface regions indicating near surface sorption mechanisms. The coal/wood-derived particles constitute only 5% of the sediment by weight but contain 62% of the total PAHs. The remaining 38% are mainly in a clay and silt fraction. PAH desorption kinetic studies on these separated fractions revealed a relatively low availability of PAHs from the coal/wood fractions and a high availability from the clay/silt fraction. Additionally, these PAH-bearing coal/wood-derived particles may be removed by density separation from heavier clay, silt, and sand.

## Introduction

Owing to the abundance of polycyclic aromatic hydrocarbons (PAHs) in sediments and to the toxic, mutagenic, and carcinogenic effects attributed to these compounds, the cleanup of PAH-contaminated sediment has drawn increasing attention (1). Though bioremediation is a potentially cost-effective treatment for PAH-contaminated sediments, a fundamental long-term issue confronting sediment bioremediation is the lack of understanding of contaminant-sediment interactions and the impacts of such interactions on the failure to achieve treatment goals (1–4). Little is known about the mechanisms of PAH and other hydrophobic organic compound (HOC) sequestration and aging in soils and sediments and the resulting effect on chemical and biological

availability (5). A major factor influencing successful sediment bioremediation is the availability of contaminants to microorganisms for degradation. However, contaminants that are strongly sorbed and not available to microorganisms may also not be available for a toxic response (6, 7). Thus, knowledge of how and where PAHs are bound to sediment material is necessary to assess the efficacy of sediment bioremediation and to correlate this knowledge with reductions in availability, mobility, and toxicity.

Three fundamentally different mechanisms that may describe sorption of PAHs on sediments are as follows: (I) surface sorption processes near the external regions of organic or inorganic particles; (II) diffusion processes leading to penetration within the interior regions of porous particles; and (III) diffusion within different types of organic matter (5, 8–13). Many diffusion-based models (14–17) assume a particle-scale diffusion process, although direct physical evidence is lacking on typical depths of penetration for contaminants in field sediments. Organic-matter diffusion models with shallow penetration depths on the order of submicron to tens of nanometers have also been proposed (9, 10, 18). However, particle-scale pore diffusion and organic matter diffusion are similar mathematically and difficult to distinguish from model fitting of desorption kinetics data (5). The problem with these conceptualizations lies in their inability to independently measure both a diffusion coefficient and a diffusional distance in field contaminated sediments. Direct measurement of HOC contaminant location on sediments at the microscale has not been possible thus far. Hence, current methods that employ macroscopic techniques for assessing sorption and sequestration of HOCs, like PAHs, on geosorbents do not provide direct information about where toxic contaminants are located, how they are associated, and what fundamental mechanisms govern their sorption. These deficiencies point to the need for improved understanding of PAH-geosorbent interactions and sequestration processes and the effect of such processes on bioavailability and toxicity (1, 5). Furthermore, an increased understanding is needed about the location and nature of PAH association in sediment that leads to their unavailability. Such knowledge could impact policy decisions for setting sediment quality criteria, defining cleanup goals, selecting appropriate treatment technologies, and establishing priorities among various environmental problems.

In this research we employed complementary microscale analytic techniques to investigate where PAHs reside in sediment and to determine the material with which they are associated. A primary technique employed in this study was microprobe laser desorption/laser ionization mass spectrometry ( $\mu\text{L}^2\text{MS}$ ), which measures PAH concentrations from a 40  $\mu\text{m}$  diameter spot (19). This technique was supplemented with Fourier transform infrared (FTIR) microspectroscopy and scanning electron microscopy with wavelength dispersive X-ray spectroscopy (SEM/WDX) to evaluate the organic and elemental components in the sediment with which PAHs are associated. A method for particle sectioning was developed that allowed the investigation of PAHs through the interior of sediment particles. The use of these novel instruments and techniques made it possible to describe the character of sorption mechanisms directly at a subparticle level. Desorption kinetic tests were used to evaluate PAH affinity for the different sediment fractions identified in this study.

\* Corresponding author phone: (650)725-9170; fax: (650)725-3164; e-mail: luthy@ce.stanford.edu.

<sup>†</sup> Department of Civil and Environmental Engineering.

<sup>‡</sup> Department of Chemistry.

## Materials and Methods

The sediment used in this study was obtained from the Milwaukee Harbor Confined Disposal Facility (CDF) operated by the Milwaukee Harbor Port Authority. These sediments originated from the Milwaukee harbor during the process of dredging to maintain waterway navigability. Concerns have been raised about the potential for release of contaminants from such CDF sites and about closure requirements, as discussed by Bowman et al. (20). The sediment was sieved through a 1/4 in. screen and stored at 4 °C until used.

**Microscale PAH Measurements.**  $\mu\text{L}^2\text{MS}$ , as described in Gillette et al. (19), was used to identify and characterize the trace distribution of PAHs on sediment particles. The first step in the  $\mu\text{L}^2\text{MS}$  analysis involves desorption of constituent molecules on a particle with a pulsed IR laser beam focused to a 40  $\mu\text{m}$  spot using a cassegrainian microscope objective. In the second step, the desorbed molecules are selectively ionized with a pulsed ultraviolet laser (266 nm), and the resulting ions are extracted into a reflectron time-of-flight mass spectrometer. Data presented here are based on multiple laser shots at different locations on particles as well as multiple shots at the same spot. To account for possible differences in PAH desorption efficiency in a particular spot, multiple laser shots were taken from a single spot until all PAHs were depleted and the signal was summed. The PAH detection limit of the  $\mu\text{L}^2\text{MS}$  instrument was estimated to be in the subattomole range. Depth of penetration of the desorption laser was assessed to be approximately 0.5–1.0 microns based on test results with PAH embedded in thin resin sections.

**Elemental Analysis.** Elemental analysis of the particle surfaces was conducted and correlated with PAH location and abundance. Measurement of the microscale elemental composition of sediment particles was performed using an SEM/WDX (Phillips XL-FEG40). The WDX analysis uses similar principles as energy-dispersive X-ray (EDX) analysis, which collects and analyzes X-rays produced when an electron beam from a SEM strikes the specimen. The WDX employs an electromechanical system that uses crystals and gas-ionization detectors to collect and analyze the X-rays, giving it higher spectral resolution and sensitivity than the traditional EDX, as well as the ability to detect soft X-rays emanating from low molecular weight elements such as boron and carbon.

**Microscale Organic Carbon Measurements.** FTIR microspectroscopy was used to discern the predominant types of sorbent carbon. FTIR microspectroscopy combines the spatial resolution of a microscope with FTIR spectral analysis making it possible to analyze IR absorbances down to a diffraction-limited spatial resolution of approximately 10  $\mu\text{m}$ . Use of synchrotron radiation provides a nearly 2 orders of magnitude brightness advantage over standard laboratory global IR sources. This work was carried out at the National Synchrotron Light Source, Brookhaven National Laboratory, using a Spectra Tech IR $\mu\text{s}$  microspectrometer connected to infrared beamline U10B. The detector used was a mercury–cadmium–telluride element with a low energy spectral sensitivity limit of 600  $\text{cm}^{-1}$  and was cooled with liquid nitrogen. A gold mirror was used for background correction. Further details of the performance of the microspectrometer are available in Carr et al. (21). These measurements were repeated at the Advanced Light Source, Lawrence Berkeley National Laboratory (IR-beamline 1.4). Transmission FTIR using bulk material formed into KBr pellets was performed using a Mattson ATI FTIR-NIR spectrometer.

**Particle Sectioning.** Sediment particles were sectioned by cryomicrotomy (Leica UltracutR) to expose the internal surface for microanalysis. Sectioning using cryomicrotomy was selected because it does not involve any contact of the

specimen with organic materials or solvents, which may adversely affect the integrity of the sample. Particles were attached to the cryomicrotome stub using a small bead of water that was then frozen by immersion in liquid nitrogen. The frozen stub was then transferred to the cryomicrotome holder and maintained at  $-150\text{ }^\circ\text{C}$  during cutting. A 2.1 mm cryo-dry, 45° diamond knife (Diatome US, Fort Washington, PA) was used to section the particles at a cutting speed of 1–2 mm/s with a cutting thickness of 0.2  $\mu\text{m}$ . A clean-cut section on the particle was obtained after approximately 500–1000 sections were shaved off the particle. After sectioning, the particles were thawed in a desiccator and mounted on brass stubs for further analysis.

**PAH Analysis by Gas Chromatography-Flame Ionization Detection (GC-FID).** PAH extraction from whole sediment was performed using three successive ultrasonic extractions (15 s on and 15 s off pulsing for a total of 3 min) with a 50:50 mixture of hexane and acetone following EPA method 3550B. The extracts were combined and cleaned using a silica gel column as outlined in EPA method 3630C. A Hewlett-Packard gas chromatograph (Model 6890) with a fused silica capillary column (HP-5, 30 m  $\times$  0.25 mm I.D.) and a flame ionization detector was used for analysis based on EPA method 8100 for PAHs. A standard EPA mixture of 16 PAH compounds obtained from Ultra Scientific was used for calibration.

**PAH Desorption Study.** PAH desorption kinetic studies were conducted using the original sediment and also separated fractions. Desorption tests followed previously used procedures (22–24). Contaminated sediment (2.0 g) and Tenax beads (0.5 g, 40–60 mesh, Suppelco, PA) were added to a 15 mL glass vial containing 10 mL of water and continuously mixed in a rotator. For desorption experiments using coal/wood-derived material, 1 g of Tenax beads and 0.5 g of sample were used to account for the higher PAH and organic carbon content in the sample. Mercuric chloride (1.0 mg) was added to the mixture to prevent any biological growth. These studies were conducted in duplicate. At sampling times, the Tenax beads were harvested by allowing the sediment to settle and the Tenax beads to float up. The Tenax beads were scooped out of the test tube and fresh Tenax beads were added. PAHs were extracted from the Tenax beads by agitating the beads in 10 mL of hexane and acetone (50:50 mixture) for 12 h and repeating two more times. The extracts were then combined and concentrated, cleaned using silica gel, and analyzed by GC-FID. Total PAH recovery based on summing PAHs in Tenax beads and in residual sample varied between 88 and 104%.

**Size and Density Separation.** Wet sieving was performed to separate the sediment into four size fractions (<63  $\mu\text{m}$ , 63–250  $\mu\text{m}$ , 250–1000  $\mu\text{m}$ , and >1000  $\mu\text{m}$ ). The larger size fractions (>63  $\mu\text{m}$ ) were composed primarily of sandy grains, coal-derived particles, and woody material. It was possible to wash off the lighter coal/wood-derived particles from the heavier sand particles by swirling with water in a beaker and draining off the entrained lighter particles giving two separate fractions which we define as “light” and “heavy”. This process was repeated several times until most of the lighter material was removed. Materials in the fine fraction (<63  $\mu\text{m}$ ) were density separated using a cesium chloride solution having a specific gravity of 1.8. Five grams of wet sediment and 40 mL of cesium chloride solution were centrifuged at 2000 rpm for 10 min in 50-mL glass centrifuge tubes. The fine coal/wood-derived particles floated to the top and were decanted off and collected in filter paper and washed with water several times. The heavy clay and silt were similarly washed several times to remove cesium chloride. Each of these size and density separated fractions were then analyzed for PAHs.

**Coal Petrography Analysis.** Coal petrography analysis of sediment particles was carried out using ASTM standard

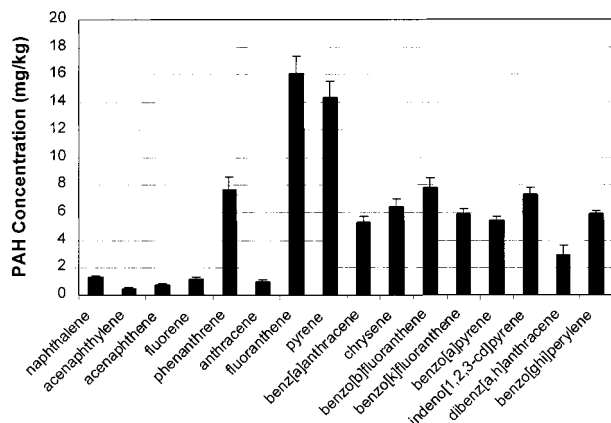


FIGURE 1. PAH distribution in the whole Milwaukee Harbor Confined Disposal Facility sediment. Error bars indicate  $\pm 1$  SD.

methods for coal analysis: D2797, D2798, and D2799.

## Results and Discussion

**Sediment PAH Concentration.** PAH extraction and analysis of the original sediment showed a total PAH concentration (EPA 16 priority pollutant PAHs) of 90 mg/kg. Figure 1 shows the distribution of the 16 measured PAH compounds. Fluoranthene and pyrene were the most abundant PAHs. The ratio of phenanthrene/anthracene was 7.6 and fluoranthene/pyrene was 1.12 indicating pyrogenic sources of the PAHs as opposed to petroleum-based sources. A phenanthrene/anthracene ratio  $< 10$  and fluoranthene/pyrene ratio  $> 1.0$  have been shown to be indicative of pyrogenic sources of PAHs (25). Coal burning and processing including gasification and coking are among the possible sources of PAHs in this sediment as indicated by Christensen and Zhang (26).

### Identification of Major Particle Classes in Sediment.

Composite sediment samples obtained from the CDF were separated into four size fractions ( $< 63 \mu\text{m}$ ,  $63\text{--}250 \mu\text{m}$ ,  $250\text{--}1000 \mu\text{m}$ , and  $> 1000 \mu\text{m}$ ) by wet sieving prior to analysis. Figure 2 is a light microscope image of the sediment particles in the  $63\text{--}250 \mu\text{m}$  size fraction. The composition of these particles was determined by elemental analysis using SEM/WDX. The most abundant class of particles in the  $> 63 \mu\text{m}$  size fractions comprises mainly silicon and oxygen and is designated as silica. The  $< 63 \mu\text{m}$  size fraction was dominated by clay particles. The second most abundant particle class within all size fractions comprised black particles containing high carbon content. These black particles were identified through petrography analysis as coal and coal-derived matter having undergone various stages of thermal treatment. Microanalysis under reflected light of polished black particles showed optically distinct coal macerals such as vitrinite, fusinite, exinite, and cutinite as indicated in Figure 3. These coal-derived particles were observed in all size fractions of the sediment down to the limit of optical resolution. Historic coal coking and gasification units located near the Milwaukee Harbor and coal shipping operations in the harbor are thought to be sources of coal in the sediment at this site (27). Particles of wood and vegetative debris, which may have originated from wood burning and the natural decay and attrition of vegetative materials, also were found in all size ranges.

These observations agree with findings reported by Griffen and Goldberg (28) that the majority of carbonaceous particles in the top 30 cm of Lake Michigan sediment are coal-based particles. Karls and Christensen (27) also reported an abundance of coal/wood-derived particles in sediments from Lake Michigan and neighboring areas. Although several studies have investigated the nature of sediment particles and proposed coal processing and wood burning as possible



FIGURE 2. Milwaukee CDF sediment particles:  $63\text{--}250 \mu\text{m}$  size fraction.

sources of PAHs in sediments, none have directly investigated the abundance of PAHs among the different sediment components.

### PAH Association with Different Sediment Components.

$\mu\text{L}^2\text{MS}$  analysis of Milwaukee CDF sediments revealed a high interparticle heterogeneity in the mass of sorbed PAHs. In a previous study, we have shown that the sediment has distinct particle types for which the surface of black particles contained much more PAHs than the surface of the silica particles (19). In this study we have characterized the black particles as coal-derived and performed parallel analyses of the location and relative abundance of PAHs, organic carbon, and elemental composition on more than 100 particles ranging in size from 20 to  $3000 \mu\text{m}$ . Figure 4 presents an example of coincident analysis of two sediment particles in the  $63\text{--}250 \mu\text{m}$  size range. The black carbonaceous particles are found to have much greater abundance of PAHs. These black particles are also high in organic carbon, which is indicated by the high IR-absorbance signal for the C-H stretching mode at  $2800\text{--}3000 \text{cm}^{-1}$ . SEM/WDX spot analysis also indicates a high concentration of elemental carbon. In comparison, the silica particles contain few PAHs and show no IR-absorbance peak at  $2800\text{--}3000 \text{cm}^{-1}$  but are high in silicon and oxygen as measured by SEM/WDX. When comparing a spot on a coal particle to a spot on a silica particle that has little or no attached organic matter, the coal particles were found to contain 2–3 orders of magnitude more PAHs on the surface. Wood-derived particles also were found to contain PAHs, but the abundance was 1 order of magnitude less, on average, than the coal-derived particles. The results of all these tests indicate that contaminating PAHs reside preferentially on the coal/wood particles. We confirmed this conclusion by particle separation and PAH analysis, which is discussed later.

**Patchy Location of PAHs on Silica Particles.** Individual sediment silica particles were found to contain heterogeneous surface distributions of clayey deposits as identified by SEM/WDX. These patchy surface deposits were high in organic carbon content as measured by IR microspectroscopy. These organic carbon locations were also relatively high in PAH concentrations based on  $\mu\text{L}^2\text{MS}$  analysis. Figure 5 displays an electron microscope image of a silica particle with a small depression on the mineral surface. IR microspectroscopy analysis of the particle revealed that this region contains organic material, as identified by the C-H stretching mode at  $2800\text{--}3000 \text{cm}^{-1}$ . The intensity of the C-H absorbance peak was mapped across the surface of the particle in the  $200 \mu\text{m} \times 200 \mu\text{m}$  square region shown in Figure 5 and is illustrated as a gray scale image on the right. The white regions indicate high organic carbon content. IR spectra of the carbon

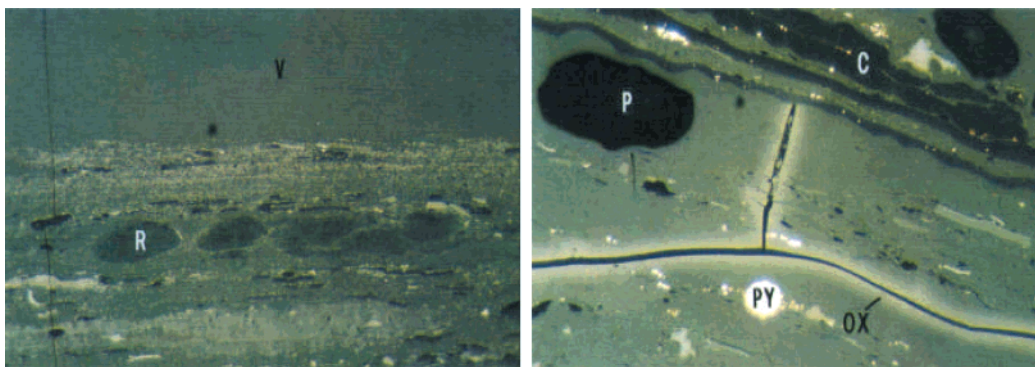


FIGURE 3. Coal petrography analysis of black particles in Milwaukee CDF sediment (V: vitrinite, R: resinite, C: cutinite, P: pore, PY: pyrite, OX: oxidized layer) (525x magnification).

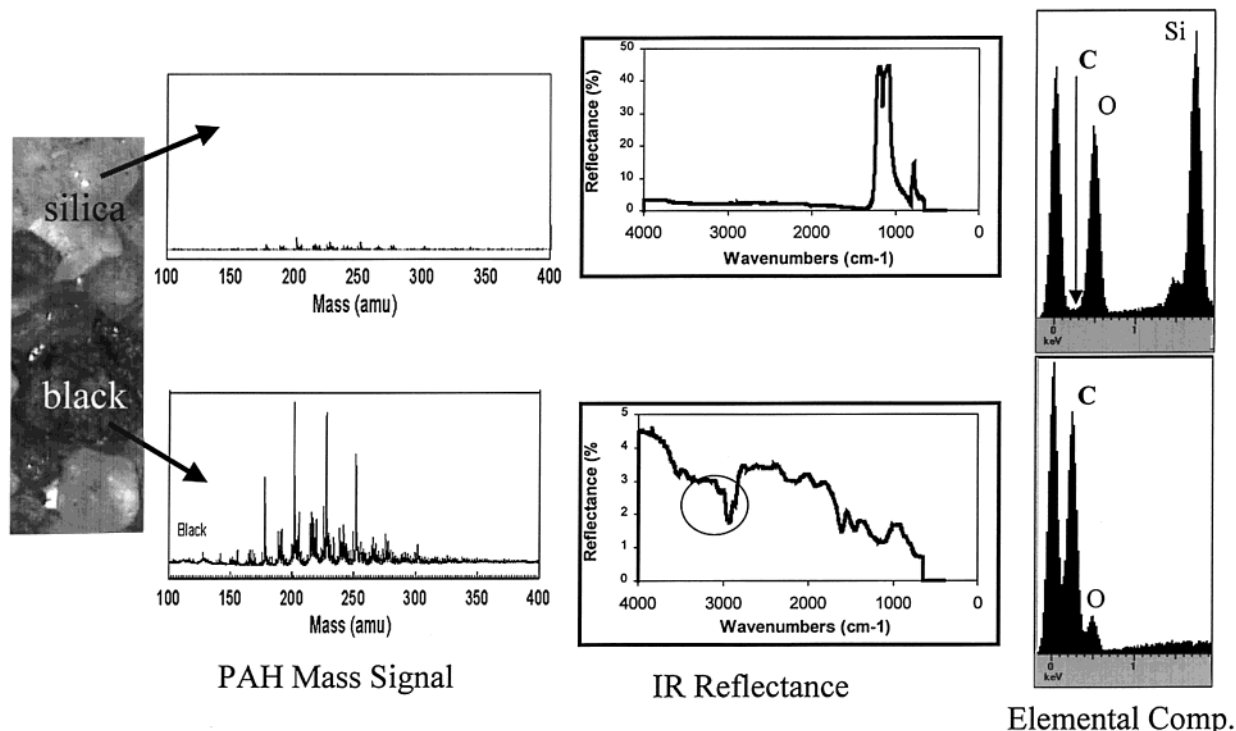


FIGURE 4. Coincident microscale analysis of PAH, organic carbon, and elemental composition of Milwaukee CDF sediment particles showing high PAH abundance on organic-carbon rich particles compared to silica particles. PAH mass signal represents the sum of 50 laser shots across the surface of a particle.

patches on silica show an aliphatic C–H abundance (2800–3000  $\text{cm}^{-1}$ ), whereas IR spectra of the coal-derived particles indicate a significant aromatic C–H component (3000–3100  $\text{cm}^{-1}$ ) in addition to an aliphatic component. This result suggests that the carbon patches on silica comprise a different carbon environment than coal-derived particles.

Figure 6 presents the subsequent  $\mu\text{L}^2\text{MS}$  spot analyses of both the organic-rich region and the surrounding silica matrix. Inspection of this figure indicates that PAHs on the silica particle lie almost exclusively within the organic matter rich region. Four spots on this particular particle were chosen for PAH analysis as indicated in Figure 5. Spots 1 and 2 were in the organic-rich region, and spots 3 and 4 were on the bare silica region. Spots 1 and 2 each contain over 100 times more PAHs than spots 3 and 4 which showed barely detectable PAHs. It is apparent that PAHs on silica particles are associated with organic carbon deposits on the particles and not bare silica regions. Additional  $\mu\text{L}^2\text{MS}$  analyses of various silica particles confirmed this characteristic pattern of PAH sorption wherein organic matter and PAHs exhibit patchy, collocated distributions.

It has been suggested previously that HOCs are partitioned into organic carbon on soils and sediments as a process of aging (29, 30). However, organic carbon can be present in soils and sediments in various forms such as humic matter particles, humic matter sorbed on mineral surfaces, vegetative debris, and products of coal and wood use and combustion. Little is known about the relative importance of these different forms of organic carbon in the sequestration of PAHs in sediments. Data in Figures 4 and 6 present direct observation of the relative abundance of PAHs associated with these different forms of sediment organic carbon.

**PAH Distribution on Particle Interior Regions.** To date, no evidence exists in the literature on direct observation of PAHs, or any other sorbed organic contaminants, on the interior of natural particles. Hence, cross-sectional analysis of the Milwaukee sediment particles was performed to understand better what role diffusion or incorporation of PAHs into the interior regions of particles might play in sequestering PAHs.

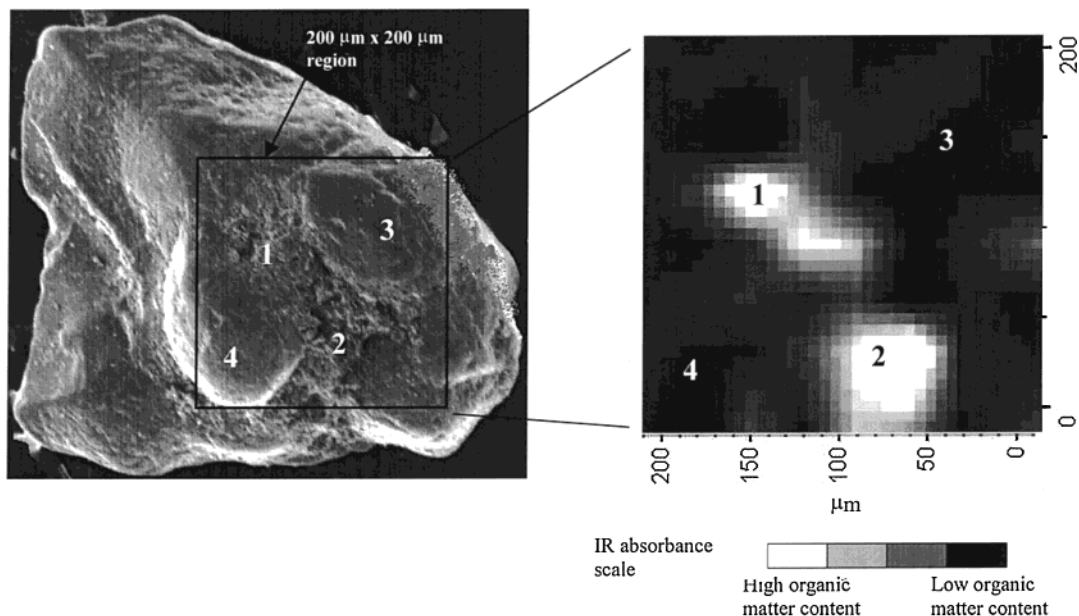


FIGURE 5. SEM image of a silica particle having patches of organic matter as indicated by the white regions in the IR mapping of C–H stretching absorbance ( $2800\text{--}3000\text{ cm}^{-1}$ ) shown in the right panel. Regions 1 and 2 also showed higher abundance of aluminum and magnesium compared to spots 3 and 4 as determined by SEM-WDX.

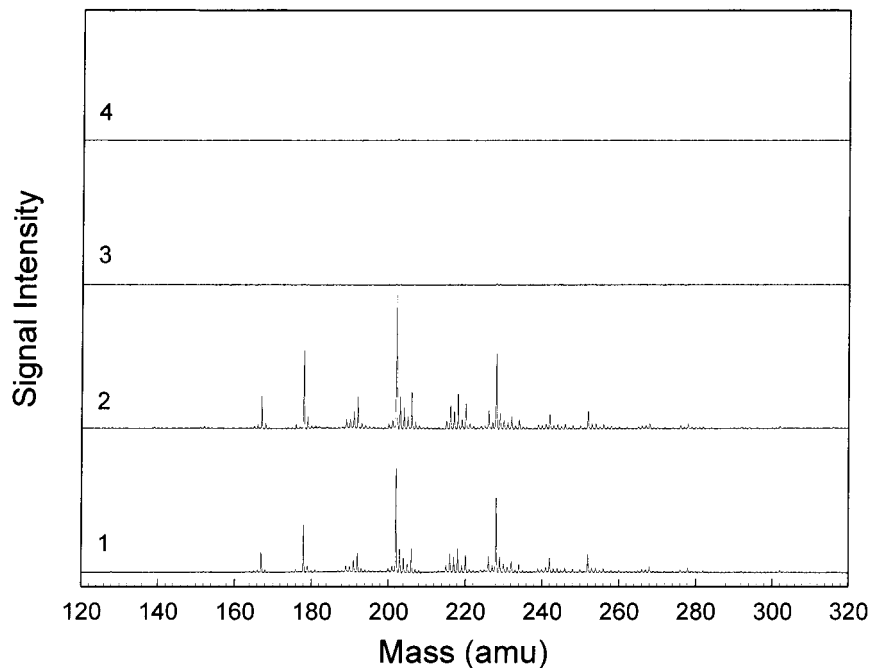


FIGURE 6. Spectra 1 and 2, resulting from  $\mu\text{L}^2\text{MS}$  analysis of PAH concentration within organic matter patches on the silica particle (spots 1 and 2 in Figure 5), show a high PAH abundance. In contrast, spectra 3 and 4, resulting from analysis of PAH concentration on bare silica region (spots 3 and 4 in Figure 5), show barely detectable PAHs. PAH signal was obtained from desorbing all PAHs from a single spot using 15 consecutive laser shots and summing the signal.

A dozen samples each of the coal-derived and silica sediment particles, approximately  $200\text{--}1000\ \mu\text{m}$  in diameter, were sectioned by cryomicrotomy and analyzed. Figure 7 shows a light microscope image of a typical coal-derived Milwaukee sediment particle after sectioning. SEM/WDX analysis revealed that the sectioned surface was abundant in elemental carbon throughout the interior. Mapping of organic carbon using FTIR microspectroscopy also revealed strong C–H stretching bands throughout the particle interior, indicating a more or less homogeneous substrate composed of organic matter.  $\mu\text{L}^2\text{MS}$  spot analysis was performed on exterior portions of the particle surface and compared to the results from interior regions. The plots in Figure 7 result

from analysis of PAH concentration at different locations across the particle transects at approximately  $50\text{-}\mu\text{m}$  intervals. It is seen that the exterior surface locations (positions 1 and 10 in Track A and 1 and 9 in Track B) contain over 30 times more PAHs than adjacent interior locations (positions 2 and 9 in Track A and 2 and 8 in Track B). For PAH analysis of the adjacent interior locations, the periphery of the desorption spot was only  $3\text{--}5\ \mu\text{m}$  from the particle section edge. By translating the desorption spot an additional  $45\ \mu\text{m}$  toward the interior of the particle, it was observed that the total PAH concentration diminished by 2 orders of magnitude compared to the exterior regions. Analysis of various coal-derived Milwaukee sediment particles showed a consistent pattern

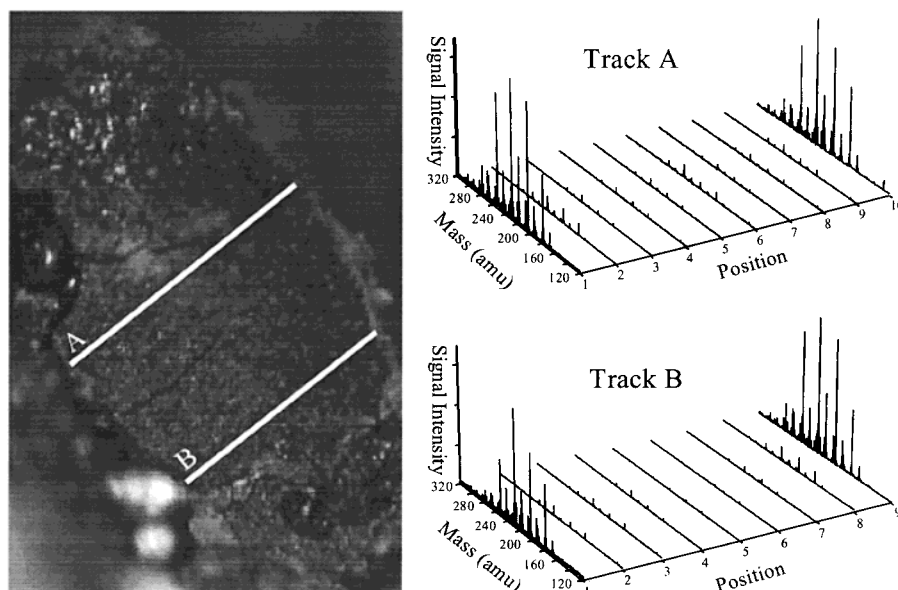


FIGURE 7. The left panel shows a sectioned surface of a coal-derived particle illustrating two linear tracks on which measurements of PAH concentrations by  $\mu\text{L}^2\text{MS}$  were performed. PAH concentration profiles measured by  $\mu\text{L}^2\text{MS}$  along tracks A and B, shown in the two plots on the right, indicate an abundance of PAHs on the near-surface regions compared to the interior regions.

of dramatic decrease in PAH concentration toward the interior. Milwaukee sediment silica particles also were sectioned and analyzed for PAHs and organic carbon. As described earlier, the surface of silica particles contain relatively few PAHs, all of which are associated with attached organic matter. Several silica particles were sectioned, and no detectable PAHs were seen in interior regions.

These direct observations suggest that a particle-scale pore diffusion conceptual model is not appropriate to describe the association of PAHs with these sediment particles, whether coal-derived or silica. It is evident that a dominant sequestration mechanism for these particular sediment particles entails near-surface sorption processes, perhaps with shallow penetration ( $<5\ \mu\text{m}$ ), as compared to incorporation throughout a porous substrate or within organic matter interior regions. Although this work is the first report of the direct observation of organic contaminant concentrations within sediment particles, some indirect evidence exists supporting shallow penetration depths of contaminants. Previous work by Pignatello et al. (18) and Brusseau et al. (9) on desorption rates of field-aged pesticides from soil showed little particle-size dependence down to the clay-size fraction, which suggested that diffusion lengths were on the order of  $1\ \mu\text{m}$  or less. Similarly, Carroll et al. (10) reported no particle size effects on PCB desorption from river sediments and suggested diffusion length scales on the order of 30 nm, which were estimated from theoretical calculations of diffusion coefficients of PCBs in humic polymers.

The complementary microscale analytical methodologies presented in this work provide direct evidence of PAH sorption on sediments at the subparticle scale and may thereby help resolve some of the contentious issues in understanding sequestration processes. This study provides direct physical evidence of preferential PAH binding to coal-derived particle surfaces, which may reduce availability and toxicity and thereby reduce contaminant risk. These results may be useful in explaining differences in availability and toxicity of PAHs in sediment particles. These issues are explored in the following measurements of PAH distribution and desorption by particle size and type.

**Separation and Analysis of Coal/Wood-Derived Particles in Sediment.** PAH-bearing coal/wood-derived particles were

separated from sand and clay to perform PAH extraction and analysis by particle size and type and for the purpose of measuring PAH availability from these components. Previous work in isolating the carbonaceous particles in sediments has involved acid digestion of mineral matter followed by chemical or thermal oxidation of organic matter (27, 31). In this work we desired to separate bulk quantities of coal/wood-derived particles without sacrificing the particle integrity or affecting the PAHs associated with such particles. Therefore, the difference in density of the coal/wood-derived particles and sand and clays was utilized to perform the separation. Figure 8a presents the sediment mass in each fraction. The heavy,  $<63\ \mu\text{m}$  size fraction comprised clays and silt and is the most abundant component in the sediment at about 60 wt %. The sum of all heavy fractions in the sediment, which includes clays, silt, and sand, constitutes about 95% of the sediment mass. The light fractions and debris constitute the remaining 5% of the sediment weight, but as shown in Figure 8b, 62% of the PAHs are associated with the lighter coal/wood-derived material and debris. Only 38% of the total PAHs are associated with the heavy sediment fraction (sand, silt, and clays), with clays and silt ( $<63\ \mu\text{m}$ ) contributing nearly all the PAHs for the heavy sediment fractions. Thus, 5% of the sediment, the coal/wood-derived material and debris, contains more than three-fifths of the total PAHs. Figure 8c shows the PAH concentration by dry mass within each fraction. The light fractions have 2 orders of magnitude higher PAH concentration than the heavier fractions. These bulk-PAH measurements support our earlier microscale observation of 2–3 orders of magnitude higher PAH concentration on coal-derived particles compared to silica. Also, the PAH concentration in the light fraction increases with decreasing size range as shown in Figure 8c. PAH concentration in the light fractions was plotted against the inverse of the average radius of the size class to assess the effect of surface area-to-volume ratio on bulk concentration. An approximate linear relationship (slope = 103.1,  $R^2 = 0.996$ ) between PAH concentration (mg/kg) and inverse of radius ( $\text{mm}^{-1}$ ) indicated a sorption mechanism possibly related to surface area. These observations support the  $\mu\text{L}^2\text{MS}$  measurements of Figures 4 and 7 showing a preponderance of PAHs on the outer surfaces of coal-derived particles.

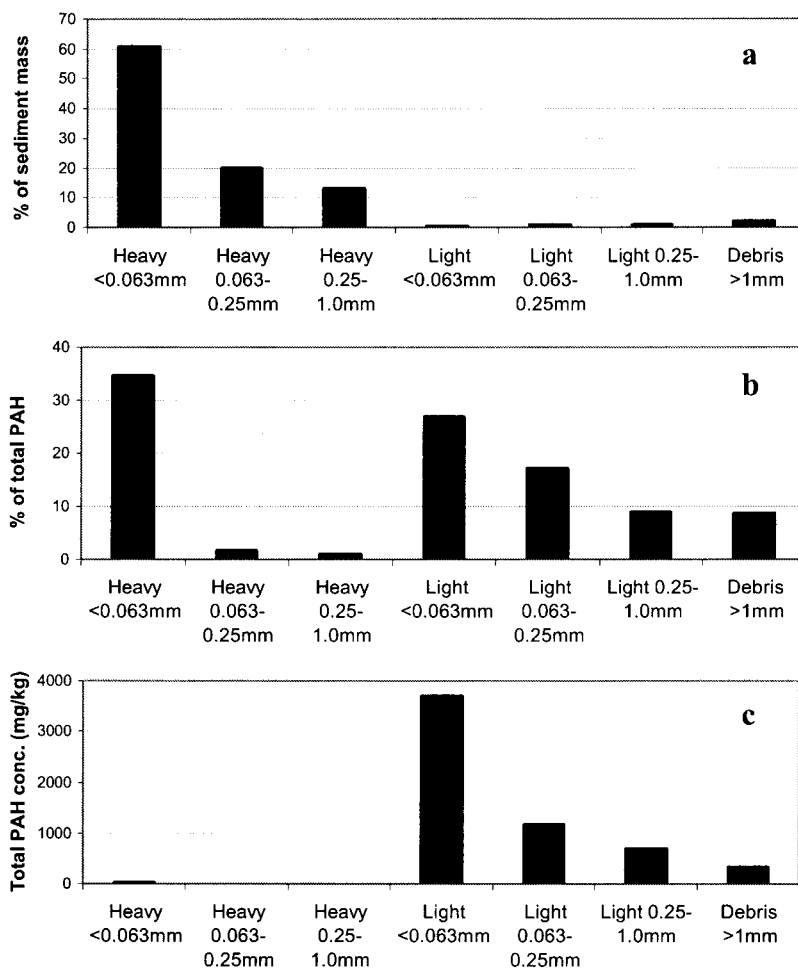


FIGURE 8. (a) Mass distribution of sediment by size and density fractions. (b) Total PAH distribution in sediment by size and density fractions (c) PAH concentration in sediment fractions by size and density.

There are several significant implications of the finding that majority of the PAHs are associated with coal derived particles. Gustafsson et al. (31) reported for Boston Harbor sediments that PAH sorption coefficients for carbonaceous residues from pyrogenic sources such as soot may be 2–3 orders of magnitude greater than that for biogenic organic matter. Similarly, Grathwohl (32) has shown that partition coefficients for HOCs on bituminous coals are approximately 2 orders of magnitude higher than that for HOCs on organic matter such as humic acids. Thus, an important implication of preferential sorption of PAHs onto coal and coal-derived materials is possible stronger affinity for PAHs and thus much less availability than for PAHs on organic matter associated with sand, silt, and clays.

Previous studies have shown the existence of an available and a relatively unavailable fraction of PAHs in aged sediments (6, 22, 23). Our findings indicate that 62% of the total PAHs are associated with coal/wood-derived particles, and this fraction may be strongly sorbed and constitute a large proportion of the unavailable PAHs. The PAHs associated with clays or organic matter on clays, silt, and sand may be less strongly sorbed and constitute a large proportion of the readily available PAH fraction.

**Desorption Kinetics Studies with Density Separated Sediment Fractions.** Desorption experiments were conducted with the various fractions to evaluate whether PAHs desorb from the different components of the sediment at different rates. Unseparated Milwaukee sediment was subjected to desorption experiments with successive Tenax additions as the PAH extractant to study the overall desorption behavior of the PAHs in the sediment. Similar desorption

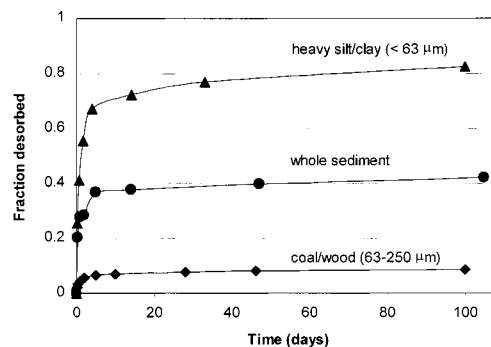


FIGURE 9. Fraction of PAH desorbed from whole Milwaukee CDF sediment (●), coal/wood-derived fraction, 63–250 μm (◆), and clay/silt fraction, <63 μm (▲). Data shown are average of duplicate measurements.

experiments were performed with the lighter coal/wood-derived fraction (63–250 μm) and the clay fraction (<63 μm) from which the lighter particles had been removed by density separation.

Figure 9 shows the average of replicate measurements carried out in the desorption experiments over a period of nearly 100 days. Data shown in Figure 9 are total PAH desorbed normalized to the initial amount of PAH in the test sample. Tests with the whole Milwaukee CDF sediment show that approximately 40% of the PAHs were released quickly and approximately 60% were strongly bound. Thus, approximately 40% of the PAHs in the whole sediment may constitute the available fraction. The PAHs associated with

the light coal/wood-derived fraction appear to be bound very strongly, as only about 8% of the PAHs in this fraction were released in 3 months. The majority of the PAHs associated with this coal/wood-derived fraction may not be bioavailable for degradation nor exhibit a highly toxic response. In contrast, desorption data from the heavier clay/silt fraction indicate a higher availability with nearly 80% of the initial PAHs in this fraction readily desorbing in 1 month.

The unavailable fraction of PAHs in sediments has for a long time hindered remediation efforts. Our findings from microscale analyses of PAH locations and characterization of particle types followed by physical separation of the PAH-laden particles have provided a better understanding of sediment-contaminant behavior that may explain low PAH availability. For Milwaukee Harbor dredged sediment, an important finding is that unavailable, strongly sorbed PAHs may largely be associated with the coal/wood-derived fraction, while the available, less strongly sorbed PAHs may largely be associated with the clay/silt fraction. The finding that the majority of unavailable PAHs are associated with a small fraction of the sediment mass that can be separated should have significant implications for sediment management and remediation. The unavailable PAH fraction in these sediments may pose less risk and therefore be present only as a contaminant and not a pollutant.

The United States Environmental Protection Agency (USEPA) has recently announced that there are too many site-specific variations in sediment composition that affect the bioavailability of contaminants in sediments to justify a national set of standards (33). Instead of numerical standards being used as legal requirements, sediment quality guidelines are being proposed by the USEPA and the United States Army Corps of Engineers that will be used as guidance in conjunction with site-specific biological tests (33). Therefore, complementary microscale measurement techniques presented in this work and others under development can provide better understanding of physicochemical mechanisms controlling site-specific bioavailability of contaminants and provide a stronger scientific basis for determining sediment quality guidelines.

### Acknowledgments

We acknowledge funding for this research from the Department of Defense through the Strategic Environmental Research and Development Program (Contract no. DACA3998K0050) and the U.S. Army Waterways Experiment Station (Contract no. DACA3997K0031). We especially thank Mr. Jeffrey W. Talley and the Environmental Laboratory of the Waterways Experiment Station for providing sediment samples and the technical collaboration, which made this research possible. Additionally, we acknowledge the Brookhaven National Laboratory, National Synchrotron Light Source and Lawrence Berkeley National Laboratory, Advanced Light Source for providing access to FTIR microspectroscopy facilities. We also thank Mr. Joseph Suhan from Carnegie Mellon University for his help with developing methods for particle sectioning.

### Literature Cited

- (1) NRC *Contaminated Sediments in Ports and Waterways, Cleanup Strategies and Technologies*; National Research Council: Washington, DC, 1997.

- (2) Wilson, S. C.; Jones, K. C. *Environ. Pollut.* **1993**, *80*, 229–249.
- (3) NRC *Alternatives for Groundwater Cleanup*; National Research Council: Washington, DC, 1994.
- (4) NRC *Innovations in Groundwater and Soil Cleanup*; National Research Council: Washington, DC, 1997.
- (5) Luthy, R. G.; Aiken, G. R.; Brusseau, M. L.; Cunningham, S. D.; Gschwend, P. M.; Pignatello, J. J.; Reinhard, M.; Traina, S.; Weber, W. J. J.; Westall, J. C. *Environ. Sci. Technol.* **1997**, *31*, 3341–3347.
- (6) Linz, D. G.; Nakles, D. V. *Environmentally Acceptable Endpoints in Soil*; American Academy of Environmental Engineers: Annapolis, MD, 1997.
- (7) Tang, J.; Carroquino, M. J.; Robertson, B. K.; Alexander, M. *Environ. Sci. Technol.* **1998**, *32*, 3586–3590.
- (8) Steinberg, S. M.; Pignatello, J. J.; Sawhney, B. L. *Environ. Sci. Technol.* **1987**, *21*, 1201–1208.
- (9) Brusseau, M. L.; Jessup, R. E.; Rao, P. S. C. *Environ. Sci. Technol.* **1991**, *25*, 134–142.
- (10) Carroll, K. M.; Harkness, M. R.; Bracco, A. A.; Balcarel, R. R. *Environ. Sci. Technol.* **1994**, *28*, 253–258.
- (11) Hatzinger, P. B.; Alexander, M. *Environ. Sci. Technol.* **1995**, *29*, 537–545.
- (12) Weber, W. J. J.; Huang, W. *Environ. Sci. Technol.* **1996**, *30*, 881–888.
- (13) Pignatello, J. J. *Environ. Sci. Technol.* **1996**, *30*, 1–11.
- (14) Wu, S.; Gschwend, P. M. *Water Resour. Res.* **1988**, *24*, 1373–1383.
- (15) Ball, W. P.; Roberts, P. V. *Environ. Sci. Technol.* **1991**, *25*, 1237–1249.
- (16) Pedit, J. A.; Miller, C. T. *Environ. Sci. Technol.* **1995**, *29*, 1766–1772.
- (17) Gong, Y.; Depinto, J. V. *Water Res.* **1998**, *32*, 2518–2532.
- (18) Pignatello, J. J.; Ferrandino, F. J.; Huang, L. Q. *Environ. Sci. Technol.* **1993**, *27*, 1263–1271.
- (19) Gillette, J. S.; Luthy, R. G.; Clemett, S. J.; Zare, R. N. *Environ. Sci. Technol.* **1999**, *33*, 1185–1192.
- (20) Bowman, D. W.; Brannon, J. M.; Batterman, S. A. *Proceedings of the 11th US Army Corps of Engineers Waterways Experiment Station Seminar*; 1996.
- (21) Carr, G. L.; Reffner, J. A.; Williams, G. P. *Rev. Sci. Instrum.* **1995**, *66*, 1490–1492.
- (22) Pignatello, J. J. *Environ. Toxicol. Chem.* **1990**, *9*, 1107–1126.
- (23) Cornelissen, G.; Van Noort, P. C. M.; Govers, A. J. *Environ. Toxicol. Chem.* **1997**, *16*, 1351–1357.
- (24) Ghosh, U.; Weber, A. S.; Jensen, J. N.; Smith, J. R. *J. Soil Contamination* **1999**, *8*, 593–613.
- (25) Budzinski, H.; Jones, L.; Bellocq, J.; Pierard, C.; Garrigues, P. *Marine Chem.* **1997**, *58*, 85–97.
- (26) Christensen, E. R.; Zhang, X. *Environ. Sci. Technol.* **1993**, *27*, 139–146.
- (27) Karls, J. F.; Christensen, E. R. *Environ. Sci. Technol.* **1998**, *32*, 225–231.
- (28) Griffen, J. J.; Goldberg, E. D. *Science* **1979**, *206*, 563–565.
- (29) Karickhoff, S. W. In *Contaminants and Sediments*; Baker, R. A., Ed.; Ann Arbor Science Pub. Inc.: Ann Arbor, MI, 1980; pp 193–205.
- (30) Chiou, C. T. In *Reactions and Movement of Organic Chemicals in Soils*; Sawhney, B. L., Brown, K., Eds.; Soil Science Society of America: Madison, WI, 1989; pp 1–29.
- (31) Gustafsson, O.; Haghseta, F.; Chan, C.; MacFarlane, J.; Gschwend, P. M. *Environ. Sci. Technol.* **1997**, *31*, 203–209.
- (32) Grathwohl, P. *Environ. Sci. Technol.* **1990**, *24*, 1687–1693.
- (33) Renner, R. *Environ. Sci. Technol.* **1998**, *32*, 306A.

Received for review September 8, 1999. Revised manuscript received February 14, 2000. Accepted February 21, 2000.

ES991032T